Electronic and magnetic properties of superlattices of graphene/graphane nanoribbons with different edge hydrogenation

A. D. Hernández-Nieves,[1,2,*] B. Partoens,[1] and F. M. Peeters[1,†]

[1]*Department of Physics, University of Antwerp, Groenenborgerlaan 171, B-2020 Antwerpen, Belgium*
[2]*Centro Atomico Bariloche, 8400 San Carlos de Bariloche, Rio Negro, Argentina*
(Received 21 May 2010; published 6 October 2010)

Zigzag graphene nanoribbons patterned on graphane are studied using spin-polarized *ab initio* calculations. We found that the electronic and magnetic properties of the graphene/graphane superlattice strongly depends on the degree of hydrogenation at the interfaces between the two materials. When both zigzag interfaces are fully hydrogenated, the superlattice behaves like a freestanding zigzag graphene nanoribbon, and the magnetic ground state is antiferromagnetic. When one of the interfaces is half hydrogenated, the magnetic ground state becomes ferromagnetic, and the system is very close to being a half metal with possible spintronics applications whereas the magnetic ground state of the superlattice with both interfaces half hydrogenated is again antiferromagnetic. In this last case, both edges of the graphane nanoribbon also contribute to the total magnetization of the system. All the spin-polarized ground states are semiconducting, independent of the degree of hydrogenation of the interfaces. The *ab initio* results are supplemented by a simple tight-binding analysis that captures the main qualitative features. Our *ab initio* results show that patterned hydrogenation of graphene is a promising way to obtain stable graphene nanoribbons with interesting technological applications.

PACS number(s): 73.22.−f, 73.22.Pr, 71.15.Mb

I. INTRODUCTION

Graphene[1] has emerged as a prospective material for nanoelectronics[2–5] and spintronics applications,[6,7] owing to the high mobility of carriers, the low-intrinsic spin-orbit interaction, as well as the low-hyperfine interaction of the electron spins with the carbon nuclei.[6] The absence of an energy band gap in graphene can be overcome by patterning graphene into nanometer size ribbons, which have been realized in recent experimental studies.[2–5] The existence of width-dependent energy bandgaps makes graphene nanoribbons (GNRs) a potentially useful structure for various semiconducting applications. *Ab initio* calculations show that zigzag GNRs are magnetic[8,9] and they become half metallic by breaking the symmetry between the left and right edges.[9–11] This can be achieved by using a different chemical termination at each edge,[9,10] or by applying an external electric field.[11]

Transport properties of GNRs depend on its edge disorder.[4] At present, controlling the shape and width of the GNR is a very challenging experimental task.[4,5] There are also experimental evidences, corroborated by *ab initio* calculations, that the zigzag edge is metastable in vacuum because it shows a planar reconstruction to lower its energy.[12] A new possibility for the fabrication of high-quality graphene nanoribbons is by selectively hydrogenating graphene or by carving GNRs on a graphane sheet.[13]

First-principles calculations predicted that graphane is a wide-gap insulator.[14,15] This novel material was synthesized recently by exposing graphene to a cold hydrogen plasma.[16] The promising properties of graphene/graphane structures have attracted recently a large interest.[13,17–19] It was shown that the energy band gaps of both zigzag and armchair graphane nanoribbons increase as the nanoribbons become narrower.[17,18] Hybrid graphene/graphane nanoribbons in vacuum where also studied from *ab initio* calculations and it

was shown that the energy band gap is dominated by the graphene section of the nanoribbon.[18] A bandgap opening in graphene, induced by the patterned absorption of atomic hydrogen onto the Moiré superlattice positions of graphene grown on a substrate, was recently found experimentally.[19] *Ab initio* calculations indicate that the observed gap opening is due to the confinement effect in the residual bare graphene regions.[19]

The edge states of graphene/graphane superlattices where recently considered in the tight-binding approximation. If the interface is oriented along a zigzag direction, edge states enhance effects related to the spin-orbit interaction.[20] The stability of graphene/graphane nanoribbons was also studied from *ab initio* calculations, and it was predicted that the graphene/graphane nanoribbons are stable down to the limit of a single carbon chain.[21]

Patterned fluoridation of graphene is another potential way for making graphene nanoribbons. Experimental evidences of graphene fluoridation was recently reported.[22,23] Graphene fluoride is a two-dimensional material that exhibits an insulating behavior similar to graphane,[22,23] which can be also used to create superlattices of graphene nanoribbons.

In this paper, we carry out spin-polarized *ab initio* calculations to study the electronic and magnetic properties of superlattices of zigzag graphene/graphane nanoribbons (ZGGNRs). We study three cases: (i) when all the interfaces between the graphene/graphane nanoribbons are fully hydrogenated, (ii) when one edge of the nanoribbons is fully hydrogenated and the other edge is half hydrogenated, and (iii) when all the interfaces of the superlattice are half hydrogenated (see Fig. 1). We found that the magnetic ground state of the ZGGNRs are semiconducting in the above three cases but the electronic and magnetic properties strongly depend on the degree of hydrogenation of the interfaces.

The calculations were performed with the QUANTUM ESPRESSO package[24] employing spin-polarized density-
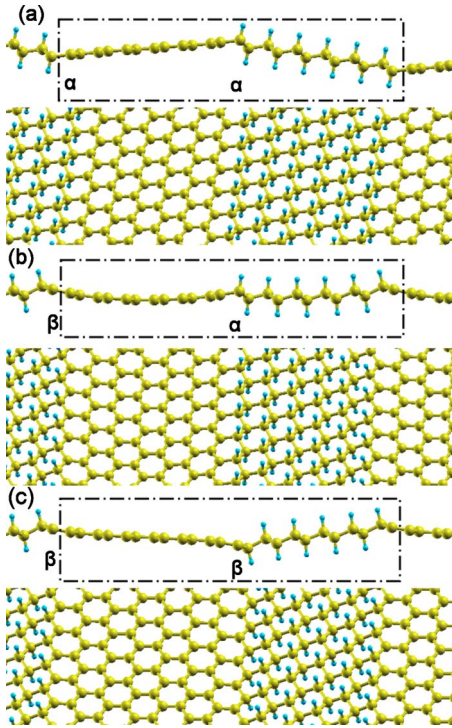
FIG. 1. (Color online) Relaxed zigzag graphene/graphane nanoribbons. (a) Both graphene/graphane interfaces are fully hydrogenated (two α interfaces), (b) one of the interfaces is fully hydrogenated and the other one is half-hydrogenated ($\alpha\beta$ nanoribbon), and (c) both interfaces are half-hydrogenated resulting in $\beta\beta$ nanoribbons. Carbon atoms are represented by large (yellow) spheres and hydrogens atoms by small (light blue) spheres. We include a side view and a perspective view of the relaxed structures for each case. The unit cells of the superlattices are shown by dashed-dotted lines in the side views.

functional theory and the Perdew-Burke-Ernzerhoff exchange-correlation functional.[25] An ultrasoft pseudopotential description of the ion-electron interaction[26] was used together with a plane-wave basis set for the electronic wave functions and the charge density, with energy cutoffs of 40 Ry and 400 Ry, respectively. The electronic Brillouin zone integration was sampled with a $16 \times 1 \times 1$ uniform k-point mesh and a Gaussian smearing of 0.01 Ry. The two-dimensional behavior of the graphene/graphane nanoribbons was simulated by adding a vacuum region of 12 Å above the graphene/graphane sheets. All the structures were relaxed using a criteria of forces and stresses on atoms of 0.001 eV/Å and 0.5 GPa, respectively.

II. RESULTS

One or both of the two carbon atoms in each unit cell of the zigzag chain at the graphene/graphane interface can be hydrogenated (see Fig. 1). The degree of hydrogenation of the zigzag chains has a very important influence on the electronic properties of the ZGGNRs. In the following, we will refer to the fully covered hydrogen interface as an α interface and to the half-covered interface as a β interface, as shown in Fig. 1. In principle, if we allow the hydrogen depo-

sition to start on a certain sublattice of graphene, it would be possible to experimentally control the degree of hydrogenation of the interfaces.

Zigzag graphene nanoribbons (ZGNR) are usually classified by the number of zigzag chains across the ribbon width.[8,11] In order to simplify the analysis, we considered superlattices of zigzag graphene/graphane nanoribbons where both, graphene and graphane nanoribbons, are six-chains wide. This means that the unit cell of Fig. 1(a) has 24 carbon and 12 hydrogen atoms. The degree of hydrogenation at the interface, and therefore the number of hydrogen atoms, decreases from Figs. 1(a)–1(c).

The interface between graphene and graphane nanoribbons is an interface between sp^2 and sp^3 bonded carbon atoms. Carbon atoms in graphene have a sp^2 hybridization and the structure stabilizes as a flat sheet. The hybridization changes from sp^2 to sp^3 in graphane due to the presence of alternating hydrogen atoms placed on both sides of the carbon plane. The sp^3 hybridization also forces nearest-neighbor carbon atoms in graphane to lie in different planes, and the resulting graphane structure is undulating.[15]

Relaxed structures of the ZGGNRs are shown in Fig. 1. All structures were fully relaxed according to the forces and stresses on the atoms by using spin-polarized calculations. When both interfaces are fully hydrogenated (two α interfaces) one side of the graphene nanoribbon is pushed up and the other side is pushed down by the graphane sp^3-bonded carbon atoms. This induces a tilt angle of 164° between adjacent graphene/graphane nanoribbons as shown in Fig. 1(a). To satisfy the conditions imposed by the sp^3/sp^2 carbon interface, the graphene nanoribbon is tilted with respect to the graphane plane but it remains flat. A similar situation occurs when both interfaces are half hydrogenated (two β-type interfaces) as shown in Fig. 1(c). In this case, the tilt angle between the graphene and graphane nanoribbons is 166.6°. When one interface is fully hydrogenated and the other one is half hydrogenated ($\alpha\beta$ superlattice), the graphene nanoribbon is pushed down at both edges by the graphane sp^3-bonded carbon atoms. This results in a curvature of the graphene nanoribbons as shown in Fig. 1(b).

It is known that a freestanding $\alpha\beta$ graphene nanoribbon is not stable. We found that by using spatially selective hydrogenation of graphene we are able to create stable $\alpha\beta$ nanoribbons. The stability of those nanoribbons was checked by allowing relaxation of the structure in our *ab initio* calculations.

We also addressed the question about the feasibility of the appearance of the zigzag interface by comparing it with the armchair interface. We prepared two supercells (one with an $\alpha\alpha$ zigzag and the other one with an armchair arrangement of atoms) forming graphene/graphane nanoribbons and containing the same number of atoms (108 atoms), 72C and 36H. We obtained only a very small energy difference of 0.002 eV/atom between the zigzag and armchair graphene/graphane nanoribbons. This value is smaller than our numerical accuracy, and it is also very small if we compare it with the thermal energy at room temperature, 0.025 eV. We can conclude that the formation energy of zigzag and armchair graphene/graphane nanoribbons are equally favorable at room temperature. This situation is different from the case
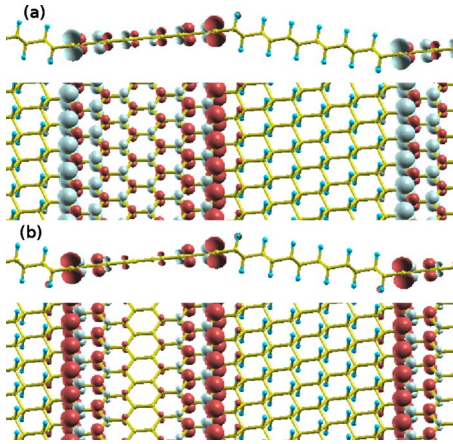
FIG. 2. (Color online) Three-dimensional (3D) graph of the spin density $(\rho_\uparrow - \rho_\downarrow)$ of the $\alpha\alpha$ zigzag graphene/graphane nanoribbon. (a) Spin density of the antiferromagnetic ground state and (b) spin density of the metastable ferromagnetic state. In both cases, the magnetization is almost completely localized in the graphene nanoribbons, and the edges of the graphane nanoribbons are only slightly magnetized. Regions with positive spin density are represented in red (dark gray) and regions with a negative spin density are shown in light blue (light gray). Isosurfaces corresponds to $(\rho_\uparrow - \rho_\downarrow) = 0.02$ $e/\text{Å}^3$, where e is the electron charge.

of freestanding nanoribbons where it was found that the zigzag edge is metastable and a planar reconstruction occurs with a lower energy.[12] This shows that graphene/graphane superlattices are a more convenient way for stabilizing zigzag graphene nanoribbons. In the following, we will only consider zigzag nanoribbons.

In calculations not shown here, we carried out structure relaxations where the volume of the unit cell is kept constant and equal to the volume of an equivalent graphane system and where only the forces between atoms are relaxed. This is equivalent to the experimental situation where graphene nanoribbons are carved in a graphane sheet with fixed borders. In this case, we found no tilt angles between the graphene and graphane nanoribbons and only a very small curvature for the $\alpha\beta$ superlattice. The electronic or magnetic properties of the system did not change in a significant way if we compare with the fully relaxed case. In the following sections, we discuss separately the electronic and magnetic properties of the ZGGNRs with different degree of hydrogenation at the interfaces.

A. Two fully hydrogenated interfaces: $\alpha\alpha$ zigzag graphene/graphane nanoribbons

We first analyze the case where both zigzag interfaces are fully hydrogenated. The ground state of the system corresponds to an antiferromagnetic (AFM) ordering between the two opposite graphene edges and a ferromagnetic (FM) ordering along the zigzag carbon chains. We will refer to this state as an AFM state. The spin density $(\rho_\uparrow - \rho_\downarrow)$ of the AFM state is represented in Fig. 2(a) while the metastable FM state (ferromagnetic ordering both between the two graphene edges and along the zigzag carbon chains) is represented in Fig. 2(b).
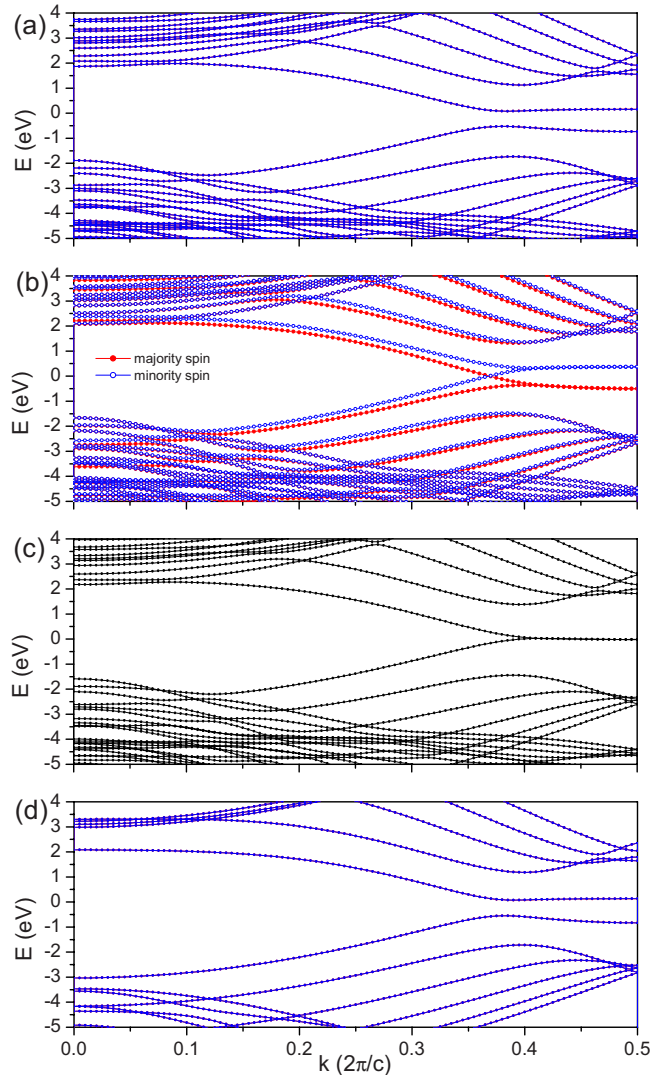

FIG. 3. (Color online) The spin-resolved band structures of the superlattice with all the interfaces fully hydrogenated, $\alpha\alpha$ ZGGNR superlattice. (a) Antiferromagnetic semiconducting ground state, (b) ferromagnetic metallic metastable state, and (c) nonmagnetic metallic metastable state. (d) The band structure of the AFM state of a hydrogen-passivated six-chains wide zigzag graphene nanoribbon. In all figures, the Fermi energy is set to zero. The energy differences of the ferromagnetic (b) and the nonmagnetic states (c) with respect to the antiferromagnetic state (a) are $E_{AFM} - E_{FM} = 8$ meV/edge atom and $E_{AFM} - E_{NM} = 35$ meV/edge atom, respectively. Spin up and spin down bands coincide in (a), (c), and (d).

The total magnetic moment and the absolute magnetic moment for the FM state are 0.59 $\mu_B/$cell and 0.95 $\mu_B/$cell, respectively (μ_B is the Bohr magneton). The AFM state has an absolute magnetic moment of 1.09 $\mu_B/$cell.

The spin density $(\rho_\uparrow - \rho_\downarrow)$ of the $\alpha\alpha$ ZGGNR are mostly concentrated in the graphene nanoribbons as shown in Figs. 2(a) and 2(b). When moving away from the interface to the center of the graphene nanoribbons, the spin density decreases faster in the FM state than in the AFM state. As a consequence, in the middle of the graphene nanoribbon, the spin density is lower in the FM state than in the AFM state.

TABLE I. Comparison between a six-chains wide freestanding zigzag graphene nanoribbon (ZGNR) and a six-chains wide $\alpha\alpha$ zigzag graphene/graphane nanoribbon ($\alpha\alpha$ ZGGNR). Energies are in millielectron volt per edge atom, bandgaps in millielectron volt, and the absolute magnetic moments (μ_{abs}) in μ_B/cell. The total magnetic moments for the FM state are 0.51 μ_B/cell and 0.59 μ_B/cell for ZGNR and $\alpha\alpha$ZGGNR, respectively.

State	$\alpha\alpha$ ZGGNR			ZGNR		
	Bandgap	ΔE	μ_{abs}	Bandgap	ΔE	μ_{abs}
AFM	578		1.09	607		1.06
FM	0.0	8	0.95	0.0	9	0.84
NM	0.0	35	0.0	0.0	36	0.0

This explains the difference of 0.14 μ_B/cell in the absolute magnetization between both magnetic states.

We also carried out *ab initio* calculations with a unit cell twice larger along the zigzag carbon chains to explore whether an antiferromagnetic ordering along the nanoribbons can be the ground state of the system. However, we found that ferromagnetic order along the nanoribbon shown in Figs. 2(a) and 2(b) gives always lower energy states.

The band structure of the ZGGNRs with the two interfaces fully hydrogenated are shown in Fig. 3. Figure 3(a) corresponds to the semiconducting AFM ground state. The FM metastable state [Fig. 3(b)] shows a metallic behavior. As the graphane nanoribbons are not spin polarized there is no significant spin density observed that can be associated with the graphane regions. The nonmagnetic metastable state is a semimetal as shown in Fig. 3(c).

The band structure of the AFM state of an equivalent six-chains wide ZGNR, thus without graphane, is represented in Fig. 3(d). We see that, near the Fermi level, the band structure of the AFM state of the superlattice [Fig. 3(a)] is very similar to the band structure of the AFM state of a graphene nanoribbon in vacuum [Fig. 3(d)]. This similarity is also observed in all the other metastable states. Thus, near the Fermi level, the band structure of the superlattice is dominated by the contribution of the graphene nanoribbons.

We carefully compared the magnetic behavior of isolated six-chains wide ZGNR with graphene nanoribbons embedded in graphane. The comparison between their electronic and magnetic properties are summarized in Table I. We found very small differences in the energy band gaps, magnetic moments, and energy differences between the different magnetic states of graphene nanoribbons in vacuum and patterned in graphane. These results show that patterning graphene nanoribbons in graphane is a promising way of obtaining zigzag graphene nanoribbons with the same electronic and magnetic properties as in vacuum.

In the four cases represented in Fig. 3, localized edge states generate flat bands near the Fermi level. Information about the spatial localization of the edge states can be obtained by analyzing the partial (or band decomposed) charge density (PCD). This is also called the integrated local density of states, which describes the density of states but space resolved, and it is useful when interpreting the data from STM experiments. In the following, we will use the term PCD.

Figure 4(a) shows the spatial localization or PCD of the edge states around E_f ($E_f \pm 0.02$ eV) for the nonmagnetic case. If we exclude the states at E_f, and do an integration from $E_f - 0.09$ eV to $E_f - 1$ eV, we see that the states become less localized, see Fig. 4(b). An interesting feature in Fig. 4(b) is that near each edge of the graphene nanoribbon only one of the two carbon sublattices makes a large contribution to the states near the Fermi level. In fact, we can appreciate from Fig. 4(b) that different carbon sublattices contribute at both edges while just in the middle of the graphene nanoribbon both sublattices contribute to the bands. The main contribution of the other carbon sublattice is located near the center of the Brillouin zone at the Γ point. These states lie at lower energies ($E_f - 2$ eV) and are entangled with the bands coming from the graphane nanoribbon.

All the above mentioned features of the band structure and the PCD of $\alpha\alpha$ ZGGNRs can be captured qualitatively with a simple tight-binding model, which results are summarized in Figs. 9(a) and 9(d) of the Appendix.

B. Superlattice with one interface fully hydrogenated and the other one half-hydrogenated: $\alpha\beta$ ZGGNRs

When one of the interfaces is half hydrogenated and the other one is fully hydrogenated the spin-polarized ground state of the system corresponds to a ferromagnetic ordering, both along the graphene/graphane interface and between the two edges of the graphene nanoribbon. Figure 5 shows the spin density for the FM ground state of the $\alpha\beta$ ZGGNR.

If we compare with an $\alpha\alpha$ ZGGNR, the absolute magnetization increases to 1.73 μ_B/cell and the total magnetization to 1.0 μ_B/cell in the $\alpha\beta$ ZGGNR. The side view of the spin density in Fig. 5 shows that the β edge of the graphane nanoribbons is also spin polarized.

The band structure of the $\alpha\beta$ ZGGNRs are shown in Fig. 6. The FM ground state shows a semiconducting behavior [Fig. 6(a)]. There are two spin-polarized flat bands near the Fermi level with a direct band gap of 0.58 eV. Ferromagnetic semiconductors have attracted a great interest since 1990s because they may lead to spintronics applications.[27] $\alpha\beta$ zigzag graphene/graphane nanoribbons may be an alternative for the well-studied diluted magnetic semiconductors (DMS) materials[27] with the fundamental difference that the system is purely two-dimensional in this case. The band structure cor-
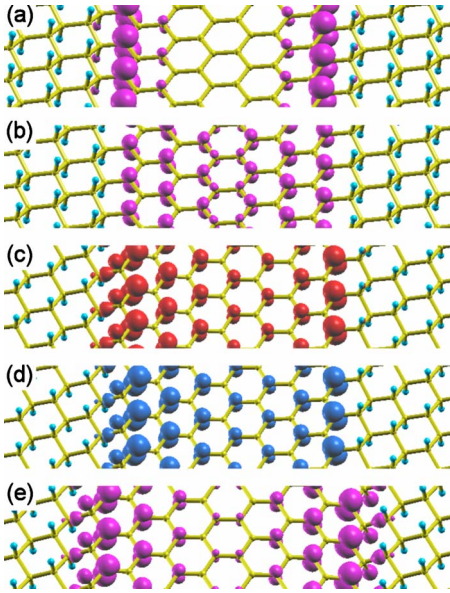
FIG. 4. (Color online) 3D graph of the PCD. (a) PCD of the nonmagnetic state of an $\alpha\alpha$ superlattice integrated in the energy window $E_f \pm 0.02$ eV, (b) the same as before but from $E_f - 0.09$ eV to $E_f - 1$ eV, (c) PCD of the majority spin states of an $\alpha\beta$ superlattice in the FM state integrated in $E_f \pm 0.7$ eV, (d) the same as (c) but for the minority spin states, and (e) PCD of the AFM state of a $\beta\beta$ superlattice from E_f to $E_f - 0.16$ eV. Red regions corresponds to majority spins (c), blue to minority spin (d), and violet means that both spins components were included in (a), (b), and (e).

responding to the nonmagnetic metastable state is represented in Fig. 6(b).

If we compare the energy difference between the magnetic and the nonmagnetic cases for the three different types of nanoribbons shown in Table II, we can see that the largest energy difference between the nonmagnetic and magnetic cases occurs for $\alpha\beta$ ZGGNRs. This indicates that the FM state of $\alpha\beta$ ZGGNRs could be even more stable than the other cases considered in this work and are summarized in Table II.

$\alpha\beta$ ZGGNRs have an extra carbon atom and, therefore, an odd number of atoms in the graphene nanoribbons (13 car-
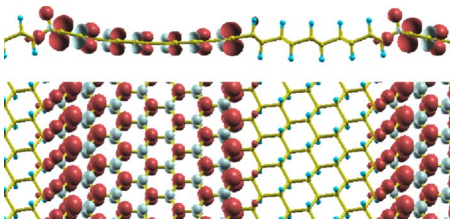

FIG. 5. (Color online) Side and perspective views of spin density of the ferromagnetic ground state of the $\alpha\beta$ ZGGNRs. Around the β interface the spin density is larger than in the α interface. The β edge of the graphane nanoribbon is also magnetized while the spin-state of the α edge is similar to Fig. 2. Regions with positive spin density are represented in red (dark gray) and regions with a negative spin density are shown in light blue (light gray). Isosurfaces corresponds to $(\rho_\uparrow - \rho_\downarrow) = 0.02 \ e/\text{Å}^3$.
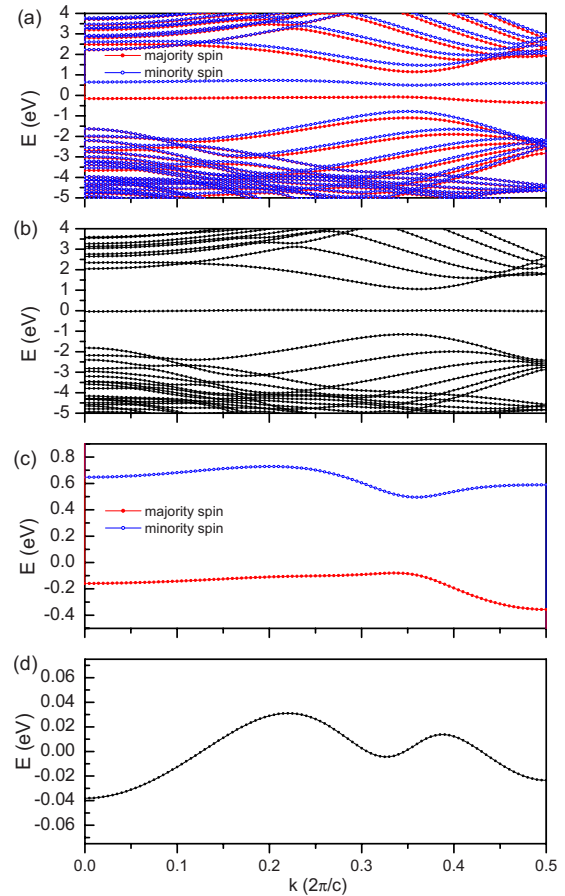

FIG. 6. (Color online) The spin-resolved band structures of the $\alpha\beta$ zigzag graphene/graphane nanoribbons. (a) ferromagnetic semiconducting ground state and (b) nonmagnetic metallic metastable state. (c) and (d) are zooms of (a) and (b) near the Fermi level, which was set to zero. The energy difference between the ferromagnetic and the nonmagnetic state is $E_{FM} - E_{NM} = 76$ meV/edge atom.

bon atoms in this case). This adds up one extra band near the Fermi level, which can be appreciated by comparing the nonmagnetic states of Figs. 3(c) and 6(b). The two bands that were previously dominating the behavior near the Fermi level in $\alpha\alpha$ ZGGNRs are now, respectively, pushed up and down in energy and very flat bands appear near the Fermi level, both for the FM ground state of Fig. 6(a) and for the nonmagnetic metastable state of Fig. 6(b).

Figures 6(c) and 6(d) are zooms of the states near the Fermi level for the FM and non magnetic states, respectively. Even when the bands are very flat, there is a small dispersion that is caused by the interaction with the graphene/graphane interfaces.

The results of the simple tight-binding model shown in Figs. 9(b) and 9(e) reproduce qualitatively the behavior of the nonmagnetic band structure. However, the band at the Fermi level is completely flat. In order to obtain dispersion in this band, we need to include an interaction with the graphane nanoribbon. This can be done by introducing an extra row of carbon atoms coupled with hydrogen as in graphane, which simulates the graphene/graphane interface. In doing so we find an extra band with a dispersion comparable to those from our *ab initio* simulations. The band width

TABLE II. Electronic and magnetic properties of graphene/graphane nanoribbons with different hydrogenation at the interfaces. Bandgaps are in millielectron volt, energy differences (ΔE) are in millielectron volt per edge atom (meV/e.a.), and the total and absolute magnetic moments (μ_t and μ_{abs}, respectively) are in units of μ_B/cell.

ZGGNR	State	Bandgap (meV)	ΔE (meV/e.a.)	μ_t (μ_B/cell)	μ_{abs} (μ_B/cell)
$\alpha\alpha$	AFM	578	0	0.0	1.09
	FM	0.0	8	0.59	0.95
	NM	0.0	35	0.0	0.0
$\alpha\beta$	FM	580	0	1.0	1.73
	NM	0.0	76	0.0	0.0
	AFM		a		
$\beta\beta$	AFM	760	0	0.0	1.92
	NM	290	37	0.0	0.0
	FM		b		

a We could not stabilize the AFM state for $\alpha\beta$ ZGGNRs. This could indicate that this state is not metastable.
b The same situation occurred for the FM state of $\beta\beta$ ZGGNRs.

does not appreciably depend on the width of the graphene nanoribbon.

More complicated tight-binding models for the case of an $\alpha\beta$ ZGGNRs where introduced in Ref. 20. However, the obtained band width[20] was four times larger than the one found with our *ab initio* results.

A very interesting feature of the PCD of the FM ground state of Figs. 4(c) and 4(d) is that only one of the carbon sublattices is contributing to the edge state. The same happens for the nonmagnetic metastable state (not shown here). This can be incorporated in a simple tight-binding model represented in Fig. 9(e). All the coefficients corresponding to one of the carbon sublattices are zero, B=D=F=H=J=L =0 in Fig. 9(e).

Notice the nearly parabolic feature of the band of the nonmagnetic state of Fig. 6(d) at $k=0$ and $k=0.5$. This allows to define and effective mass (m_{eff}) for the electrons, in this case $m_{eff}=5.77m_e$ for $k=0$ and $m_{eff}=3.22m_e$ for $k=0.5$, where m_e is electron rest mass.

C. Superlattice with the two edges half hydrogenated: $\beta\beta$ zigzag graphene/graphane nanoribbons

We consider now the case of the $\beta\beta$ superlattice represented in Fig. 1(c). The spin-polarized ground state is the AFM state as was also the case in the $\alpha\alpha$ superlattice. Figure 7 shows the spin density for the AFM ground state of the $\beta\beta$ ZGGNR. Both edges of the graphane nanoribbon contributes to the spin polarization of the system. This can be better appreciated in the side view at the top of Fig. 7. The absolute magnetic moment of the AFM state is 1.92 μ_B/cell, almost twice larger than in the AFM state of the $\alpha\alpha$ ZGGNR (1.09 μ_B/cell).

Figure 8(a) shows the band structure of the AFM ground state of the $\beta\beta$ ZGGNR and the nonmagnetic metastable state is shown in Fig. 8(b). Both are semiconducting states while the energy band gap of the AFM state (0.76 eV) is larger than in the nonmagnetic case (0.29 eV). It is interest-

ing to note that even when we have a nonmagnetic state with a band gap there is a transition to a magnetic state by further increasing the band gap. The properties of both states are summarized in Table II.

The partial charge density graph of the AFM phase near the Fermi level obtained from E_f to $E_f-0.16$ eV shows that the edge states of the $\beta\beta$ superlattice extend also to the edge of the graphane nanoribbon as shown in Fig. 4(e). The edge states decay more rapidly in the graphane nanoribbon than in the graphene region when we move away from the interface.

The qualitative features of the $\beta\beta$ ZGGNRs are also captured by the tight-binding model of the Appendix as can be appreciated from Figs. 9(c) and 9(f). Figure 9(f) also correlates with the *ab initio* PCD of Fig. 4(e). This is discussed in more detail in the Appendix. We see that the different carbon sublattices contribute differently near each edge. This situation is similar to the case we explained before for the $\alpha\alpha$ ZGGNRs.

III. CONCLUSIONS

The degree of hydrogenation of the graphene/graphane interface has an important influence on the electronic and magnetic properties of the zigzag graphene/graphane nanoribbons. This parameter could be controlled experimentally to tune the band gap and the magnetic properties of graphene/graphane superlattices.

We found that independent of the degree of hydrogenation of both interfaces the ground state of the system is semiconducting. However, the band structure near the Fermi level changes dramatically due to the contribution of the edge states in the three different superlattices. While the ground state of the system is antiferromagnetic in $\alpha\alpha$ and $\beta\beta$ ZGGNRs, it is ferromagnetic for $\alpha\beta$ ZGGNRs.

Our results show that $\alpha\alpha$ ZGGNRs are a promising way to obtain stable graphene nanoribbons with similar electronic and magnetic properties as freestanding zigzag nanoribbons. The basic properties of freestanding zigzag graphene edges
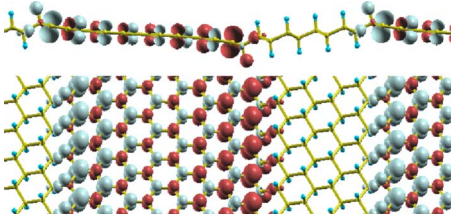
FIG. 7. (Color online) Side and perspective views of the 3D graph of the spin density of the antiferromagnetic ground state of the $\beta\beta$ graphene/graphane nanoribbons. The spin-polarized regions extend to include both edges of the graphane nanoribbon. Regions with positive spin density are represented in red (dark gray) and regions with a negative spin density are shown in light blue (light gray). Isosurfaces corresponds to $(\rho_\uparrow - \rho_\downarrow) = 0.02$ $e/\text{Å}^3$.

are preserved when the system binds on both edges to insulating graphane regions. We also found that the energy difference between zigzag and an armchair graphene/graphane nanoribbons is very small, the energy difference per atom is one order of magnitude smaller than the thermal energy at room temperature. This means that the formation energies of zigzag and armchair graphene/graphane nanoribbons are equally favorable at room temperature. This situation is different from the case of freestanding nanoribbons where it was found that the zigzag edge is metastable because it exhibits a planar reconstruction that decreases its energy.[12] Then, graphene/graphane superlattices seem a promising way to solve structural and stability problems faced by freestanding nanoribbons.

We proposed a single atom thick ferromagnetic semiconductor in $\alpha\beta$ zigzag graphene/graphane nanoribbons. It may
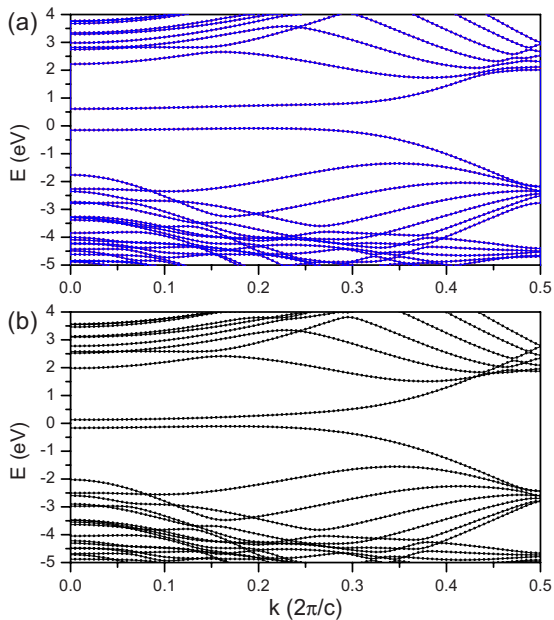

FIG. 8. (Color online) The spin-resolved band structures of a $\beta\beta$ ZGGNRs. (a) Antiferromagnetic semiconducting ground state and (b) nonmagnetic semiconducting metastable state. The Fermi energy is set to zero. The energy difference between the antiferromagnetic and the nonmagnetic state is $E_{\text{AFM}} - E_{\text{NM}} = 37$ meV/edge atom. The spin-polarized bands coincide in both cases.
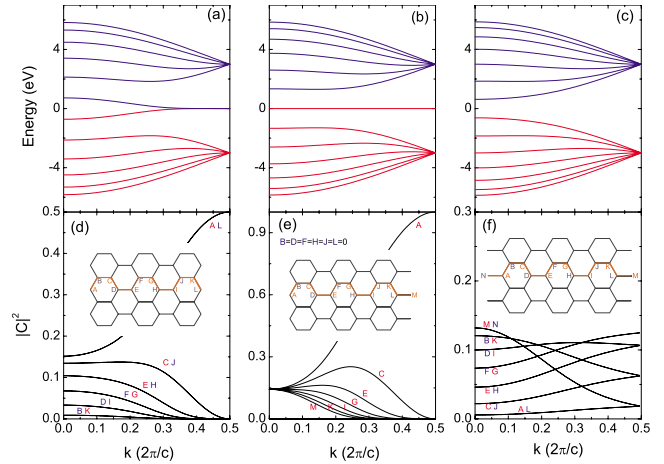

FIG. 9. (Color online) Band structures for graphene nanoribbons with (a) two α edges containing 12 carbon atoms in the unit cell, (b) one α and one β edges and 13 atoms in the unit cell, and (c) two β edges with 14 atoms in the unit cell. The Fermi energy is set to zero. (d), (e), and (f) show the values of the coefficients $|C_i|^2$, for all atoms in the unit cell, of the highest valence band corresponding to (a), (b), and (c), respectively.

be an alternative for the well-studied DMS materials[27] with the fundamental difference that the system is purely two-dimensional in this case. Diluted semiconductors are of interest from both fundamental and applied points of view, and may soon lead to spintronics devices with new functionalities.[27]

$\alpha\beta$ ZGGNRs can also be analyzed in a more general framework. In order to render a ZGNR half metallic, the symmetry between the left and right edges of the zigzag nanoribbon should be broken. For example, in Ref. [11] this was done by applying an electric field to the system, in Ref. [9] this was done by adding a Klein's edge to one side of the nanoribbon, and in Ref. [10] the two zigzag edges were terminated with different terminal groups, such as NO_2 and CH_3. The present work shows that in graphene/graphane superlattices, this could be achieved by controling the degree of hydrogenation at the two edges.

From Fig. 6(c) we can appreciate that the ferromagnetic ground state of $\alpha\beta$ ZGGNRs is almost a half metal. As the Fermi level is in between two spin-polarized bands, with little charge doping the Fermi level can be shifted either to the spin-up or spin-down band. This could be used in a potentially interesting electronic device. So half-metalicity in $\alpha\beta$ ZGGNRs can be achieved not with the help of an external electric field as in Ref. [11] but with charge doping, which could offer new technological alternatives.

It is known that the width of the nanoribbons has a strong influence on the bandgap of the graphene nanoribbons[8,11] as well as on the band gap of the graphane nanoribbons.[17,18] Both, the width of the graphene nanoribbons and the level of hydrogenation at the interface can be used to control the electronic and magnetic properties of graphene/graphane nanoribbons. While the width of the graphane region can be used to control the energy window where graphene and graphane bands entangle.

Most of the qualitative features obtained in our *ab initio*

calculations can be explained with a simple tight-binding model incorporated in the Appendix. This shows that the present results can be qualitatively extrapolated to other type of superlattices where graphene nanoribbons are patterned by selective absorption of different atoms. Another interesting candidate, with similar or even better characteristics as graphane is graphene fluoride, a two-dimensional material that has been recently synthesized.[22,23]

APPENDIX: TIGHT-BINDING MODEL OF GRAPHENE NANORIBBONS

In order to obtain extra insight in the presented *ab initio* results for the electronic structure of graphene/graphane nanoribbons, we construct a simple tight-binding model. Here we focus only on the graphene part of the nanoribbon. To construct the tight-binding Hamiltonian we consider a tight-binding Bloch function per atom in the primitive cell

$$\psi_{\vec{k}}^i(\vec{r}) = \frac{1}{\sqrt{N}} \sum_{i}^{N} \varphi(\vec{r} - \vec{r}_i) \exp(i\vec{k} \cdot \vec{r}_i), \quad (A1)$$

where $\vec{r}_i$ is the position of a carbon atom in the primitive cell, and φ denotes the p_z-like atomic wave function of a carbon atom. N is the number of considered unit cells. All carbon atoms are positioned on the (unrelaxed) honeycomb lattice as in pure graphene. We consider a zigzag nanoribbon with the same number N_c of carbon atoms in the unit cell as in the graphene/graphane nanoribbons studied in this paper. For two α edges $N_c=12$, for a nanoribbon with one α and one β edge $N_c=13$, and $N_c=14$ in case of two β edges. The total eigenfunction is then given by

$$\Psi_{\vec{k}}(\vec{r}) = \sum_{i=1}^{N_c} C_i \psi_{\vec{k}}^i(\vec{r}). \quad (A2)$$

This results in symmetric $N_c \times N_c$ tight-binding Hamiltonians with the following nonzero off-diagonal elements (with only nearest neighbor interactions) (1) nanoribbon with two α edges

$$H(2i+1, 2i+2) = \gamma \cos(kc) \quad \text{with } i = 0, \dots, 5, \quad (A3)$$

$$H(2i+2, 2i+3) = \gamma \quad \text{with } i = 0, \dots, 4, \quad (A4)$$

(2) nanoribbon with one α and one β edge

$$H(2i+1, 2i+2) = \gamma \cos(kc) \quad \text{with } i = 0, \dots, 5, \quad (A5)$$

$$H(2i+2, 2i+3) = \gamma \quad \text{with } i = 0, \dots, 5, \quad (A6)$$

(3) nanoribbon with two β edges

$$H(2i+1, 2i+2) = \gamma \quad \text{with } i = 0, \dots, 6, \quad (A7)$$

$$H(2i+2, 2i+3) = \gamma \cos(kc) \quad \text{with } i = 0, \dots, 5. \quad (A8)$$

We have chosen the on-site energy as the zero of energy $\int \varphi^*(\vec{r} - \vec{r}_i) H \varphi(\vec{r} - \vec{r}_i) d\vec{r} = 0$, and the tight-binding parameter γ is defined in the usual way

$$\gamma = \int \varphi^*(\vec{r} - \vec{r}_i) H \varphi(\vec{r} - \vec{r}_i - \vec{R}) d\vec{r} \equiv 3 \text{ eV} \quad (A9)$$

where $\vec{R}$ is the vector connecting an atom with its nearest neighbor.

The band structures of the zigzag graphene nanoribbons obtained within this tight-binding model are shown in Fig. 9. Figures 9(a)–9(c) show results for the $\alpha\alpha$, $\alpha\beta$, and $\beta\beta$ cases, respectively. The Fermi energy lies at $E_F=0$. The obtained spectra agree qualitatively with the corresponding *ab initio* ones for the nonmagnetic graphene/graphane nanoribbons in Figs. 3(c), 6(b), and 8(b). Note the absence of dispersion of the band at $E=0$ for the $\alpha\beta$ graphene nanoribbon [Fig. 9(b)], in contrast to the *ab initio* result where a small dispersion was observed, see Fig. 6(d). This dispersion is a consequence of the graphane edge, which is not taken into account in the present tight-binding model.

Below each band structure of Fig. 9, we plot the corresponding coefficients $|C_i|^2$ from Eq. (A2) of the highest valence band eigenstate. Each curve is labeled by a letter indicating the corresponding atom in the nanoribbon unit cell. Figure 9(d) shows that in case of an $\alpha\alpha$ nanoribbon, the highest valence band state is located at both edges of the nanoribbon, represented by the carbon atoms A and L. The next most important contribution is not located at carbon atoms B and K but at atoms C and J. Note that these two atoms (C and J) belong to different sublattices, and that C and A (and also J and L) belongs to the same sublattice. The results of Fig. 9(d) can be correlated with the *ab initio* results of the PCD represented in Figs. 4(a) and 4(b).

On the other hand, for the case of an $\alpha\beta$ nanoribbon [Fig. 9(b)], the dispersionless band at the Fermi level is entirely built up from atoms that belong to one sublattice. The contributions coming from the other sublattice given by the coefficients B, D, F, H, J, and L are all zero. This is also the case for the ferromagnetic ground state of the $\alpha\beta$ nanoribbon as can be seen in the integrated local density of states of Figs. 4(c) and 4(d).

The case of a nanoribbon with two β edges is similar to the $\alpha\alpha$ nanoribbon. The highest valence band is again built up from the edge atoms M and N, see Fig. 9(f). While the contribution from the neighboring atoms belonging to the other sublattice (atoms A and L, or C and J) is again rather small. The present tight-binding model can be extended to describe the magnetic properties of the system, for example, by using the Hubbard model, as was discussed in Ref. 9.

*alexande@cab.cnea.gov.ar

†francois.peeters@ua.ac.be

[1] K. S. Novoselov, A. K. Geim, S. V. Morozov, D. Jiang, Y. Zhang, S. V. Dubonos, I. V. Grigorieva, and A. A. Firsov, Science **306**, 666 (2004).

[2] M. Y. Han, B. Özyilmaz, Y. Zhang, and P. Kim, Phys. Rev. Lett. **98**, 206805 (2007).

[3] X. Li, X. Wang, L. Zhang, S. Lee, and H. Dai, Science **319**, 1229 (2008).

[4] M. Y. Han, J. C. Brant, and P. Kim, Phys. Rev. Lett. **104**, 056801 (2010).

[5] L. Jiao, X. Wang, G. Diankov, H. Wang, and H. Dai, Nat. Nanotechnol. **5**, 321 (2010).

[6] N. Tombros, C. Jozsa, M. Popinciuc, H. T. Jonkman, and B. J. van Wees, Nature (London) **448**, 571 (2007).

[7] V. M. Karpan, G. Giovannetti, P. A. Khomyakov, M. Talanana, A. A. Starikov, M. Zwierzycki, J. van den Brink, G. Brocks, and P. J. Kelly, Phys. Rev. Lett. **99**, 176602 (2007).

[8] Y. W. Son, M. L. Cohen, and S. G. Louie, Phys. Rev. Lett. **97**, 216803 (2006).

[9] K. Kusakabe and M. Maruyama, Phys. Rev. B **67**, 092406 (2003).

[10] Er-jun Kan, Z. Li, J. Yang, and J. G. Hou, J. Am. Chem. Soc. **130**, 4224 (2008).

[11] Y. W. Son, M. L. Cohen, and S. G. Louie, Nature (London) **444**, 347 (2006).

[12] P. Koskinen, S. Malola, and H. Häkkinen, Phys. Rev. B **80**, 073401 (2009).

[13] A. K. Singh and B. I. Yakobson, Nano Lett. **9**, 1540 (2009).

[14] S. Lebègue, M. Klintenberg, O. Eriksson, and M. I. Katsnelson, Phys. Rev. B **79**, 245117 (2009).

[15] J. O. Sofo, A. S. Chaudhari, and G. D. Barber, Phys. Rev. B **75**, 153401 (2007).

[16] D. C. Elias, R. R. Nair, T. M. G. Mohiuddin, S. V. Morozov, P. Blake, M. P. Halsall, A. C. Ferrari, D. W. Boukhvalov, M. I. Katsnelson, A. K. Geim, and K. S. Novoselov, Science **323**, 610 (2009).

[17] Y. Li, Z. Zhou, P. Shen, and Z. Chen, J. Phys. Chem. C **113**, 15043 (2009).

[18] Y. H. Lu and Y. P. Feng, J. Phys. Chem. C **113**, 20841 (2009).

[19] R. Balog *et al.*, Nature Mater. **9**, 315 (2010).

[20] M. J. Schmidt and D. Loss, Phys. Rev. B **81**, 165439 (2010).

[21] V. Tozzini and V. Pellegrini, Phys. Rev. B **81**, 113404 (2010).

[22] S. H. Cheng, K. Zou, F. Okino, H. R. Gutierrez, A. Gupta, N. Shen, and P. C. Eklund, J. O. Sofo, and J. Zhu, Phys. Rev. B **81**, 205435 (2010).

[23] J. T. Robinson, J. S. Burgess, C. E. Junkermeier, S. C. Badescu, T. L. Reinecke, F. K. Perkins, M. K. Zalalutdniov, J. W. Baldwin, J. C. Culbertson, P. E. Sheehan, and E. S. Snow, Nano Lett. **10**, 3001 (2010).

[24] P. Giannozzi *et al.*, J. Phys.: Condens. Matter **21**, 395502 (2009).

[25] J. P. Perdew, K. Burke, and M. Ernzerhof, Phys. Rev. Lett. **77**, 3865 (1996).

[26] D. Vanderbilt, Phys. Rev. B **41**, 7892 (1990).

[27] T. Jungwirth, J. Jairo Sinova, Masek, J. Kucera, and A. H. MacDonald, Rev. Mod. Phys. **78**, 809 (2006).